Integration of multiple physical behaviours into a geometric tolerancing approach

Laurent Pierre, Denis Teissandier, Jean-Pierre Nadeau

Integration of multiple physical behaviours into a geometric tolerancing approach

L. Pierre[(1)], D. Teissandier[(2)], J.P. Nadeau[(3)]
(1), (3): TREFLE UMR 8508, Arts et Métiers ParisTech,
Esplanade des Arts et Métiers, 33405 Talence Cedex, France
(2): LMP UMR 5469, Université de Bordeaux,
351, Cours de la Libération, 33405 Talence Cedex, France
laurent.pierre@bordeaux.ensam.fr

Abstract
The performance of a helicopter engine depends essentially on the performance of the high-pressure turbine, closely correlated with the rotor/stator clearance at the tip of the blades. The engine's thermodynamic cycle causes elastic or plastic strains on some of the high-pressure turbine components, causing considerable geometric variations, some of which are irreversible.

In this article we propose to integrate the notion of behaviour into the evaluation of clearance in a high-pressure turbine by defining the physical phenomena that are influential during certain operational phases and more generally over the lifetime of the turbine. Modelling the variations in the geometric deviations of the parts and the contacts is based on deviation hulls and clearance hulls.

Keywords:
Tolerancing analysis, flexible parts, thermomechanic, behaviour, lifecycle, helicopter engine.

1 INTRODUCTION

Controlling the behaviour and the energy yield of helicopter engines for each of their different operational regimes is clearly essential in order to guarantee that the desired power is achieved. One way to improve the performance of these turboshaft engines is to optimise the energy yield of the different constituent components, and in particular to control clearance between the tips of the high-pressure turbine blades and the stator.

In this article we propose a method that will take into account different behaviours in order to characterise the physical phenomena that are influential during certain phases in the operational cycle.

In the first part, three behaviours are introduced for the system studied: behaviour I, where the system is new and the parts are at 20°C; behaviour II where some components in the system are subject to thermal flux, creating thermomechanical strains; behaviour III at 20°C, subsequent to behaviour II, where certain parts retain the memory of earlier plastic strains. In part two we show how changes in the contacts between the different behaviours and strains in the parts themselves are taken into account when modelling the dimension chains by operations on the hulls (Minkowski sum and intersection). In part three, we present an application of this work to a sub-unit of a high-pressure helicopter engine turbine. Lastly, after describing the main conclusions, we present future developments for this work.

2 TAKING INTO ACCOUNT SEVERAL BEHAVIOURS IN 3D DIMENSION-CHAINS

Three different behaviours are considered when modelling the operating cycle of a system (see figure 1):

- behaviour I: the system has just been assembled and has not yet been operational. All the parts are at 20°C and are considered to be infinitely rigid.

- behaviour II: some parts of the system that have been subjected to thermal flows undergo thermomechanical strains. These strains are then taken into account in the 3D dimension-chains.

- behaviour III: the system is at 20°C. Some parts that have been subjected to thermal flows for a specified duration t during behaviour II have undergone thermomechanical strains, which can create plastic strains. These plastic strains, if any exist, are then taken into account in the 3D dimension-chains.

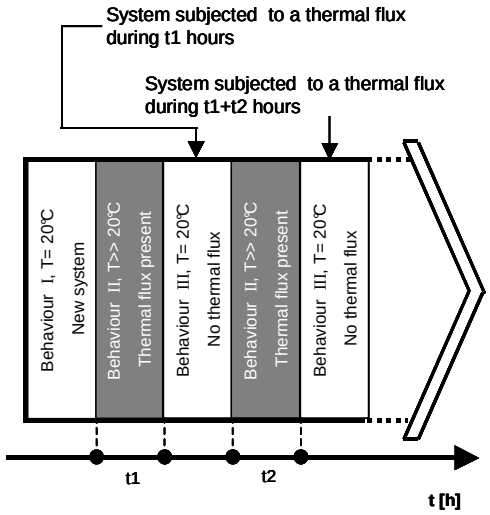

Figure 1: Operational cycle.

In this article, deviation hulls [1] are used to define the tolerated limits of the geometric defects of a part (defined by a specification), and clearance hulls to define the accepted limits of relative displacement between two surfaces in contact (defined by a clearance level), [2].

The concept of hull introduced by [3] is also developed in [4], [5] and [6].

Studies which integrate strains on the parts caused by the assembly process are currently underway: [7], [8] and [9].

2.1 Behaviour I: new system, temperature: 20°C

Let us consider the system shown in figure 2, consisting of two parts 1 and 2 in contact via a cylindrical pair joint along **x** and a ball and plane pair joint along **x**. The surface j of the part i is indicated by i,j.

One functional condition FC limiting translation d along **y** of the cylindrical surface 1,1 in relation to the axis of surface 2,1 at point A is to be fulfilled. This FC is defined in the following equation: $d_{min} \le d \le d_{max}$ (1)

Thus $\mathfrak{D}_{1,1/2,1}$ is the deviation hull characterising the relative displacement of the axis of the cylindrical surface 1,1, in relation to the axis of surface 2,1 at point A.

We transferred the FC to parts 1 and 2 in order to determine the ISO geometrical specifications [10], [11] , [12] that guaranteed that the functional condition FC was fulfilled [13], [14]: see figure 2.

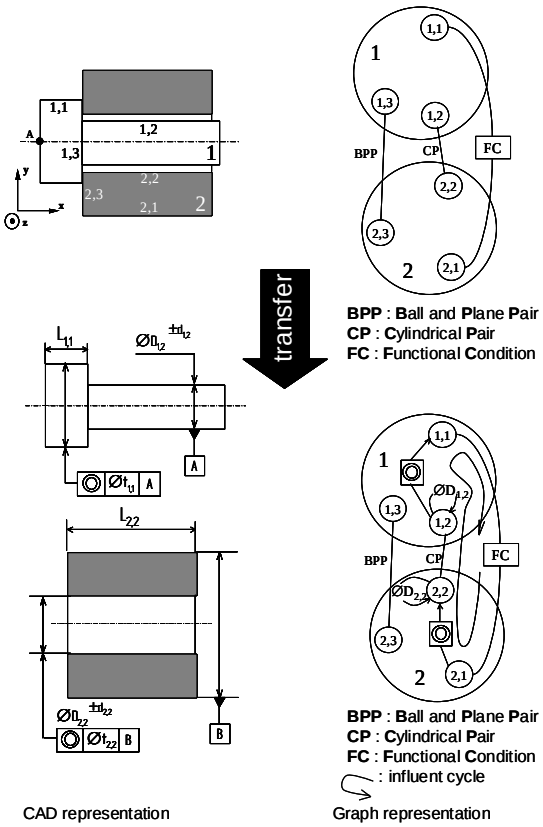

Figure 2: Transfer of FC

To simplify expression of the hulls, we study the limits of defects admissible in 2D modelling in plane $(A,\mathbf{z})$. The relative translation deviations between surfaces 1,1 and 1,2, at point A along **y** are expressed thus: $\varepsilon_{A,1,1/1,2y}$. The relative rotation deviations between surfaces 1,1 and 1,2 along **z** are expressed thus: $\rho_{1,1/1,2z}$.

At point A we can construct the deviation hulls $\mathfrak{D}_{1,1/1,2}$ and $\mathfrak{D}_{2,2/2,1}$ of the coaxialities of parts 1 and 2 respectively between surfaces 1,1 and 1,2 and surfaces 2,1 and 2,2 (see figure 3).

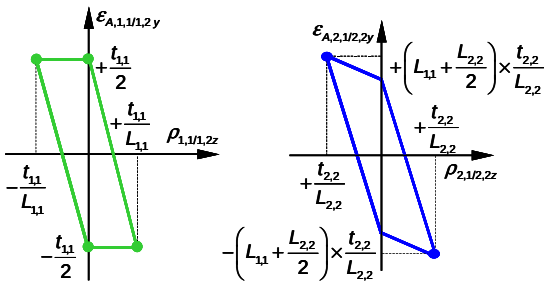

Figure 3: Deviation hulls $\mathfrak{D}_{1,1/1,2}$ and $\mathfrak{D}_{2,2/2,1}$ modelling respectively the coaxialities of surfaces 1,1 and 1,2 and 2,2 and 2,1 at point A.

Next, the clearance hull $\mathfrak{D}_{1,2/2,2}$ of the cylindrical pair joint 1,2/2,2 between parts 1 and 2 at point A can be constructed: see figure 4.

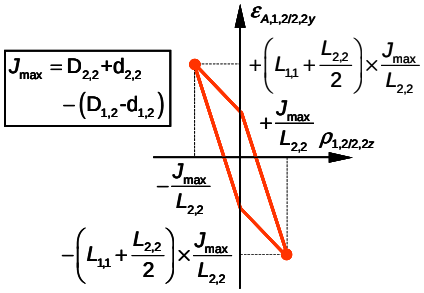

Figure 4: Clearance hull $\mathfrak{D}_{1,2/2,2}$ of joint 1,2/2,2 at point A.

Lastly, using the Minkowski sum (2) we are able to deduce hull $\mathfrak{D}_{1,1/2,1}$ (see figure 5).

$$\mathfrak{D}_{1,1/2,1} = \mathfrak{D}_{1,1/1,2} + \mathfrak{D}_{1,2/2,2} + \mathfrak{D}_{2,2/2,1} \quad (2)$$

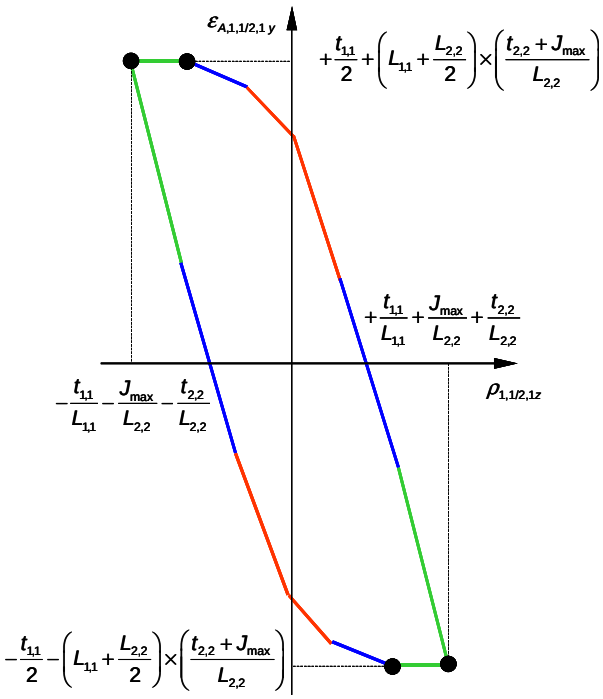

Figure 5: Minkowski sum illustrating the deviation hull $\mathfrak{D}_{1,1/2,1}$ at point A in behaviour I.

2.2 Behaviour II: system subjected to thermal flux

Consider figure 6 which describes the system studied in behaviour II. By hypothesis, part 2 remains inflexible: only part 1 undergoes thermomechanical strain. These thermomechanical strains are the result of a steep

temperature gradient along direction **y** in part 1. The result is a camber in part 1: see figure 6.

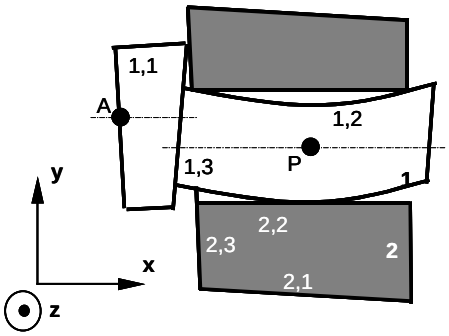

Figure 6: Behaviour II.

The cambering of part 1 within part 2 eliminates all degrees of freedom in the joint between surfaces 1,2 and 2,2. Clearance between parts 1 and 2 becomes null. Clearance hull $\mathfrak{D}_{1,2/2,2}$ is reduced to a point at the origin of the hull area: see figure 7.

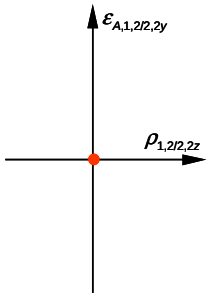

Figure 7: Clearance hull $\mathfrak{D}_{1,2/2,2}$ at point A in behaviour II.

The thermomechanical strain in part 1 results in the translation of the deviation hull $\mathfrak{D}_{1,1/1,2}$ defined in §2.1: see figure 8.

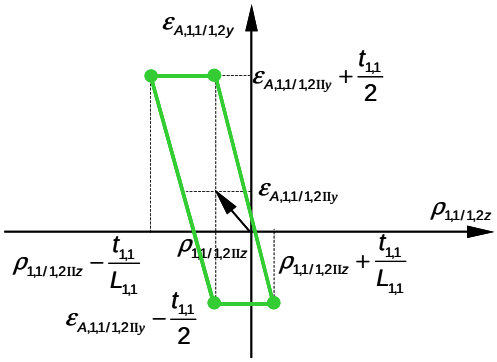

Figure 8: Deviation hull $\mathfrak{D}_{1,1/1,2}$ at point A in behaviour II.

The Minkowski sum (2) describes hull $\mathfrak{D}_{1,1/2,1}$ which is shown graphically for behaviour II in figure 9.

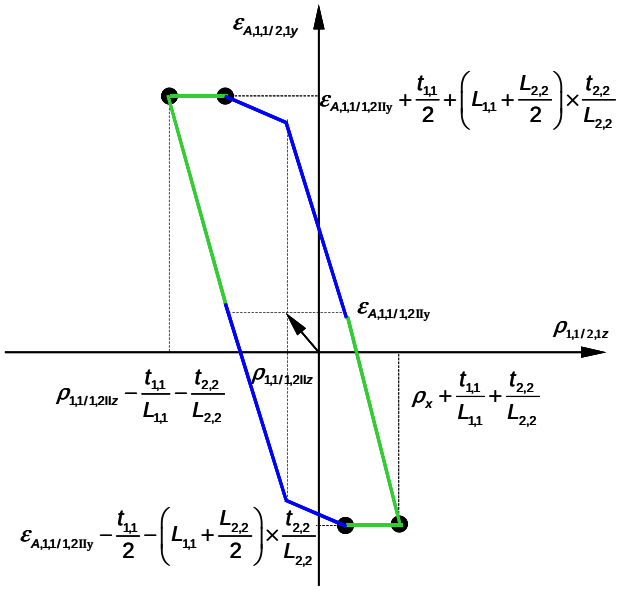

Figure 9: Minkowski sum illustrating deviation hull $\mathfrak{D}_{1,1/2,1}$ at point A in behaviour II.

2.3 Behaviour III: system at 20℃ previously subjected to thermal flux for X hours

Now we consider figure 10. Part 1 has undergone thermomechanical strain in the context of behaviour II for a specified time of X hours, and has not returned to its initial state. It undergoes a state of plastic strain called a decambering phenomenon, which is then taken into account in the 3D dimension-chains.

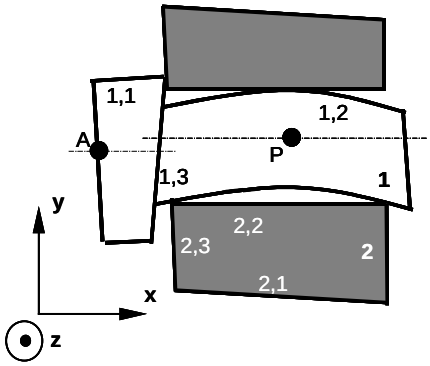

Figure 10: Behaviour III.

By hypothesis, the plastic strain in part 1 maintains null clearance in the joint 1,2/2,2.

Moreover, the decambering of part 1 modifies the deviation hull of this part at point A defined in §2.1 via translation: see figure 11.

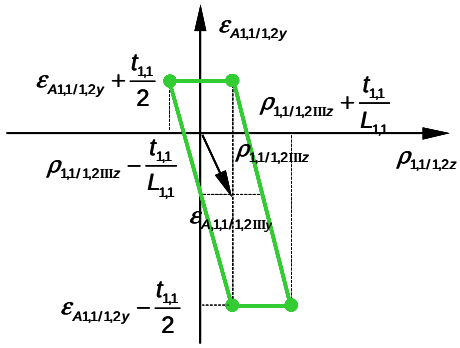

Figure 11: Deviation hull $\mathfrak{D}_{1,1/1,2}$ at point A in behaviour III.

The Minkowski sum for the deviation hulls of parts 1 and 2 and for the clearance hull between parts 1 and 2 in behaviour III is illustrated in figure 12.

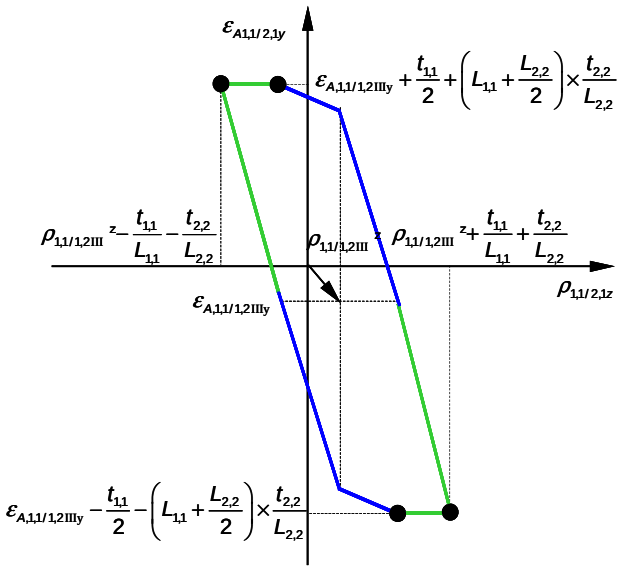

Figure 12: Minkowski sum illustrating deviation hull $\mathfrak{D}_{1,1/2,1}$ at point A in behaviour III.

Table 1 summarises the different results obtained for behaviours I, II and III in figures 5, 9 and 12 respectively in order to fulfil the FC.

Behaviour I	$+\frac{t_{1,1}}{2}+\left(L_{1,1}+\frac{L_{2,2}}{2}\right)\times\left(\frac{t_{2,2}+J_{max}}{L_{2,2}}\right)\le d_{max}$ $-\frac{t_{1,1}}{2}-\left(L_{1,1}+\frac{L_{2,2}}{2}\right)\times\left(\frac{t_{2,2}+J_{max}}{L_{2,2}}\right)\ge d_{min}$
Behaviour II	$\varepsilon_{A,1,1/1,2IIy}+\frac{t_{1,1}}{2}+\left(L_{1,1}+\frac{L_{2,2}}{2}\right)\times\frac{t_{2,2}}{L_{2,2}}\le d_{max}$ $\varepsilon_{A,1,1/1,2IIy}-\frac{t_{1,1}}{2}-\left(L_{1,1}+\frac{L_{2,2}}{2}\right)\times\frac{t_{2,2}}{L_{2,2}}\ge d_{min}$
Behaviour III	$\varepsilon_{A,1,1/1,2IIIy}+\frac{t_{1,1}}{2}+\left(L_{1,1}+\frac{L_{2,2}}{2}\right)\times\frac{t_{2,2}}{L_{2,2}}\le d_{max}$ $\varepsilon_{A,1,1/1,2IIIy}-\frac{t_{1,1}}{2}-\left(L_{1,1}+\frac{L_{2,2}}{2}\right)\times\frac{t_{2,2}}{L_{2,2}}\ge d_{min}$

Table 1: Synthesis of results of FC transfer.

3 APPLICATION TO A HIGH-PRESSURE TURBINE

3.1 Description of the turbine

The turbine is made up of two sub-units: a rotor (consisting of the part numbered 5) and a stator (consisting of the parts numbered 1, 2, 3 and 4) in a turning pair joint along **x** by the intermediary of a ball bearing numbered 6 and a cylindrical roller bearing numbered 7: see figure 13. Part 5 has a revolution shape where the largest diameter corresponds to the diameter of the heads of the blades. Clearance at the top of the blade between the vanes of part 5 and part 1 of the stator is defined as the difference in diameter between parts 1 and 5: see figure 13.

In order to maximise turbine power, this clearance should be minimised while still ensuring that in all turbine operational phases part 5 does not come into contact with part 1.

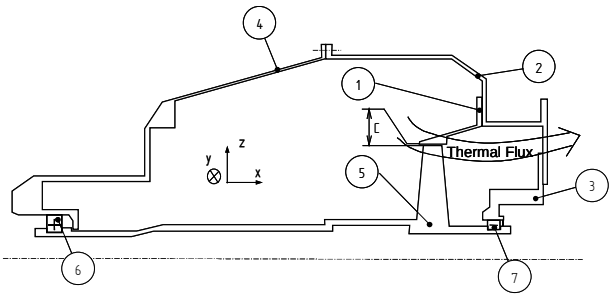

Figure 13: Simplified geometric model of a high-pressure turbine.

When the turbine is operational, a flux of hot gases (about 1000℃) is created in the combustion chamber (not shown in figure 13) which results in strain on parts 1, 3 and 5: see figure 13. In this application, we restrict our study to a sub-unit of the turbine made up of parts 1 and 2: see figure 14. The functional condition ensuring control of clearance C at the top of the blades between the rotor and the stator (see figure 13) corresponds to an alignment FC of the axes of surfaces 1,8 and 2,8: see figure 14.

FC is defined in equation (3) where e represents the distance between the axes of surfaces 1,8 and 2,8 in a direction orthogonal to **x** at point A:

$$e_{min} \le e \le e_{max} \qquad (3)$$

In this example, the thermomechanical strains in part 1 are taken into account solely when operational. Part 2 is considered to be infinitely rigid and geometrically perfect: see figure 14.

The specifications required to satisfy the FC in the three different behaviours defined in §2 are studied in turn. First, the turbine is modelled in behaviour I where only manufacturing defects and clearance in the different contacts are taken into account. Next, behaviour II is considered, where strains due to the flux of hot gases from the combustion chamber are also integrated, at a point where the turbine is functioning in a stationary regime. Finally, in a third phase, we study behaviour III after the turbine has been functioning for X hours, when only plastic strains caused by the thermomechanical strains from behaviour II are taken into account.

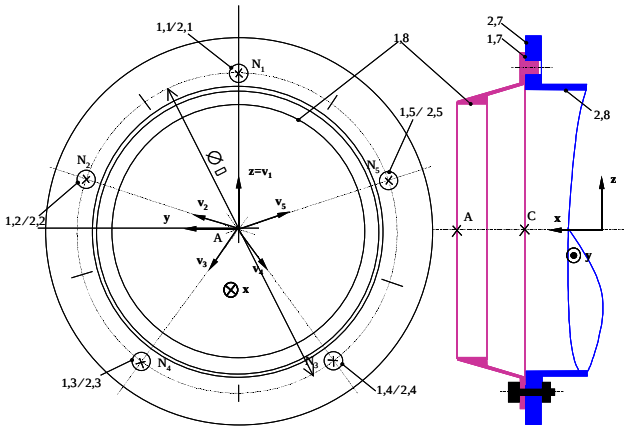

Figure 14: Sub-unit of high-pressure turbine.

3.2 Behaviour I: new turbine, temperature: 20℃

Part 1 is positioned via a support plane contact with part 2, by the intermediary of surfaces 1,7 and 2,7. Contacts between surfaces 1,1/2,1; 1,2/2,2; 1,3/2,3; 1,4/2,4; 1,5/2,5 modelled by ball and cylinder pair joints, complete the positioning between these two parts. Five clamping screws ensure that parts 1 and 2 are held in place. The graph of the joints corresponding to the system described

in figure 14 is shown in figure 15 with the parameters of the different joints.

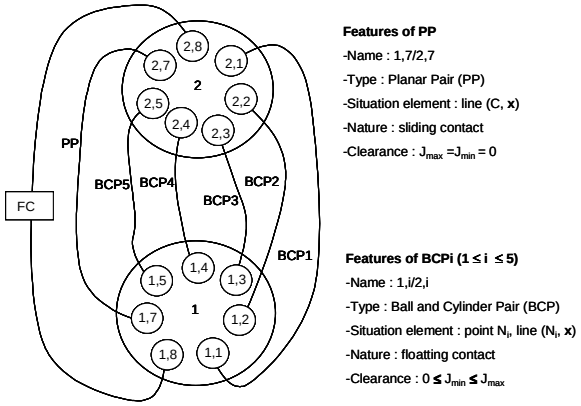

Figure 15: Graph of joints.

The CD datum reference frame on part 2 is defined in the same way as for part 1. The primary surface designated C corresponds to surface 2,7. The secondary surface designated D corresponds to the group of 5 surfaces 2,1 to 2,5.

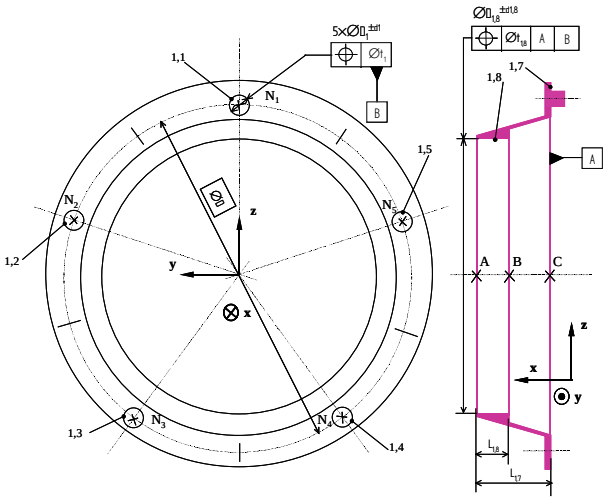

Figure 16: Drawing showing definition of part 1.

The hull describing the displacement limits of surface 1,8 in relation to surface 2,8 is expressed in the following Minkowski sum:

$$\mathfrak{D}_{1,8/2,8} = \mathfrak{D}_{1,8/AB} + \mathfrak{D}_{AB/CD} \qquad (4)$$

$\mathfrak{D}_{1,8/AB}$ is the deviation hull characterised by the location of surface 1,8 in relation to datum reference frame AB. $\mathfrak{D}_{AB/CD}$ is the clearance hull defined by the support plane joint (1,7/2,7) and the five ball and cylinder pair joints (1,i/2,i). Hull $\mathfrak{D}_{AB/CD}$ is formalised by the intersection of the clearance hulls of the joint between surfaces 1,7/2,7 and the five joints 1,i/2,i:

$$\mathfrak{D}_{AB/CD} = \mathfrak{D}_{1,7/2,7} \cap \left(\mathfrak{D}_{1,1/2,1} \cap \mathfrak{D}_{1,2/2,2} \cap \mathfrak{D}_{1,3/2,3} \cap \mathfrak{D}_{1,4/2,4} \cap \mathfrak{D}_{1,5/2,5}\right) \qquad (5)$$

For each slug maximal clearance J_{max} which is the difference between the maximum diameter of the hole and the minimum diameter of the shaft, corresponds to the most unfavourable configuration for the FC. The clearance hull $\mathfrak{D}_{AB/CD}$, resultant of the intersection of the clearance hulls for the five ball and cylinder pairs and the support plane joint, is shown in figure 17, in 2D modelling in plane $(A,\mathbf{x})$.

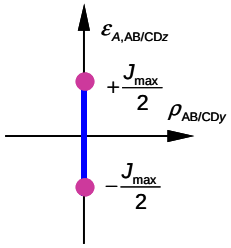

Figure 17: Clearance hull $\mathfrak{D}_{AB/CD}$ at point A.

The deviation hull $\mathfrak{D}_{1,8/AB}$ is defined at point A. This clearance characterising the location specification (see figure 16) is shown in figure 18.

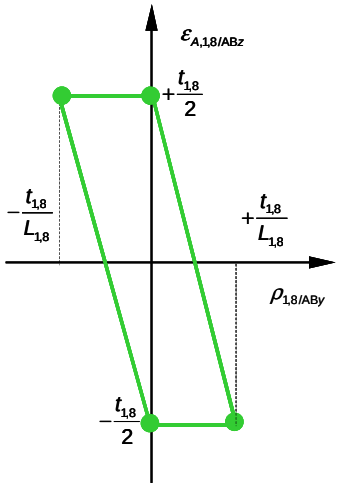

Figure 18: Deviation hull for location of surface 1,8 at point A.

The Minkowski sum defined in equation (4) is represented in figure 19.

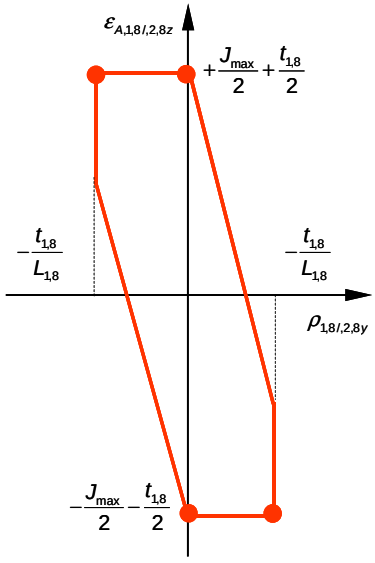

Figure 19: Hull $\mathfrak{D}_{1,8/2,8}$ at point A in behaviour I.

From this we can deduce in particular expression (6), formalising respect for the worst case FC in behaviour I.

$$\left.\begin{aligned} e_{max} &\geq +\frac{t_{1,8}}{2}+\frac{J_{max}}{2} \\ e_{min} &\leq -\frac{t_{1,8}}{2}-\frac{J_{max}}{2} \end{aligned}\right\} \qquad (6)$$

3.3 Behaviour II: turbine subjected to thermal flux (flux of hot gases at 1000 °C)

The thermomechanical strains induced by a flux of gases from the combustion chamber illustrated in figure 13 should be integrated into the dimension chains verifying that the FC are respected.

As described in §2.2, the nature of the contacts and the clearances may evolve from one behaviour to another [15].

A preliminary thermomechanical study was carried out to determine changes in the contacts. The thermal marginal conditions were provided by an expert engineer working in this field. They consisted of two fluxes: a convection flux due to the flux of hot gas from the combustion chamber, situated on the internal face of part 1; a cooling convective flux on the external face of part 1: see figure 20.

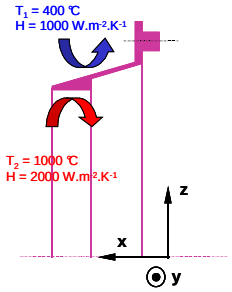

Figure 20: Thermal marginal conditions.

The only mechanical marginal conditions considered were the contact conditions of the support plane joint 1,7/2,7. This enabled us to carry out an initial analysis on the behaviour of surfaces 1,1 to 1,5.

This initial thermomechanical study shows that the radial displacement of the slugs is much greater than the maximal clearances present in each BCP type joint. Hence the nature of the contact between the five ball and cylinder pair joints changes from floating to fixed.

Moreover, the strain on part 1 adds a forced contact to each BCP type joint along direction $\mathbf{v}_i$: see figure 21.

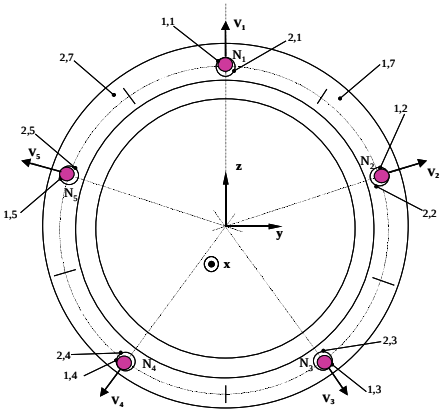

Figure 21: Radial displacement of the slugs.

For this reason clearance hull $\mathfrak{D}_{AB/2,8}$ is a point centred on the origin, given that the distribution of the slugs is angularly equidistant: see figure 22.

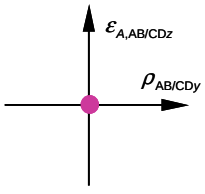

Figure 22: Clearance hull $\mathfrak{D}_{AB/CD}$ at point A.

Thermomechanical analysis of part 1 was carried out with the thermal marginal conditions defined in figure 20 and with the mechanical marginal conditions that conformed to the parameters of the different joints in behaviour II. From the strain on surface 1,8 from thermomechanical stresses we were able to determine the results obtained for figure 11 using Samcef software.

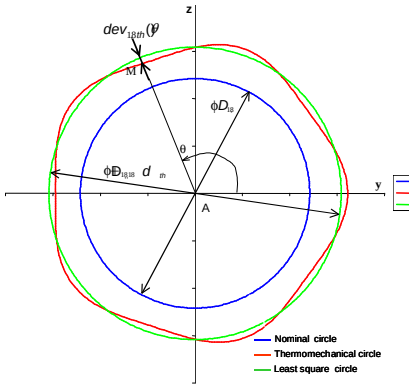

Figure 23: Thermomechanical strain of surface 1,8 in plane $(A,\mathbf{x})$.

Three results in particular were characteristic of the strain in plane $(A,\mathbf{x})$ see figure 23:

- the translation deviation at point A in the centre of the least square circle in relation to the centre of the nominal circle: $\breve{}_{A,1,8/2,8th}$

- the diameter of the least square circle of the deformed section: $D_{1,8th} = D_{1,8} + d_{1,8th}$

- the deviation in the form of the deformed section: $dev_{1,8th}(\theta)$

The thermomechanical distortion of surface 1,8 is not axisymmetrical.

Using a similar process to that used in §2.2, figure 24 shows a representation of hull $\mathfrak{D}_{1,8/2,8}$ characterising the displacement limits of surface 1,8 in relation to surface 2,8 at point A.

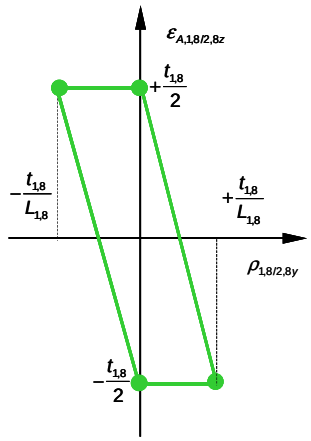

Figure 24: Hull $\mathfrak{D}_{1,8/2,8}$ at point A in behaviour II.

Expression (7) formalising fulfilment of the worst case FC condition in behaviour II can easily be deduced from figure 24.

$$\left.\begin{aligned} e_{max} &\geq +\frac{t_{1,8}}{2} \\ e_{min} &\leq -\frac{t_{1,8}}{2} \end{aligned}\right\} \qquad (7)$$

For behaviour II, equation (8) shows the translation deviation $b_{1,8}(\theta)$ of a point on cylindrical surface 1,8 in relation to its nominal position.

$$b_{1,8}(\theta) = \varepsilon_{A,1,8/2,8z} + \frac{D_{1,8} + d_{1,8th} \pm d_{1,8}}{2} + dev_{1,8th}(\theta) \qquad (8)$$

3.4 Behaviour III: turbine at 20°C after functioning for X hours

The gas fluxes from the combustion chamber during behaviour II (see §2.3) lead to plastic strains when the turbine is at rest and when the temperature of all the parts is 20°C.

The geometric deviations caused by these plastic strains are quantified by taking tridimensional measurements from part 1 after the turbine has been dismantled.

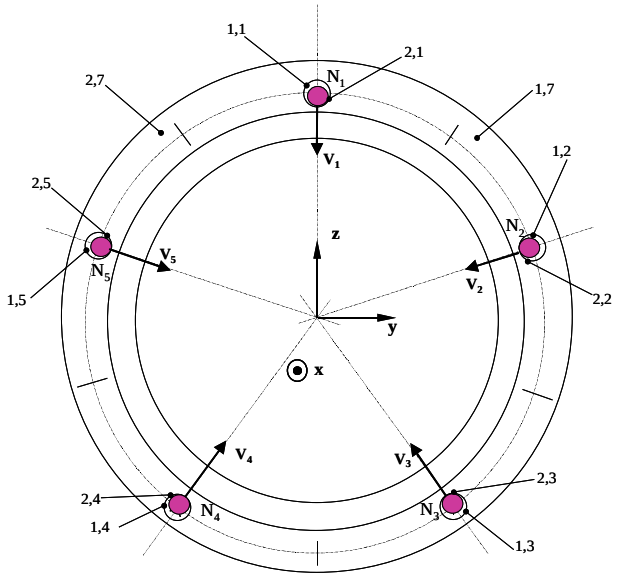

Figure 25: Radial displacement of the slugs.

Changes in the clearances in the five ball and cylinder pair joints can be checked by a simple visual inspection of the parts. The plastic strain of part 1 adds a forced contact to each BCP type joint along direction $\mathbf{v}_i$: see figure 25.

As a result, clearance hull $\mathfrak{D}_{AB_i\,2,8}$ is a point centred on the origin, given that the distribution of the slugs is angularly equidistant: see figure 26.

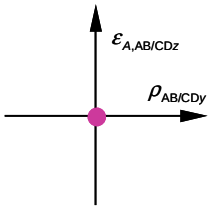

Figure 26: Clearance hull $\mathfrak{D}_{AB/CD}$ at point A.

The plastic strain of surface 1,8, determined by tridimensional metrology, is shown in figure 27.

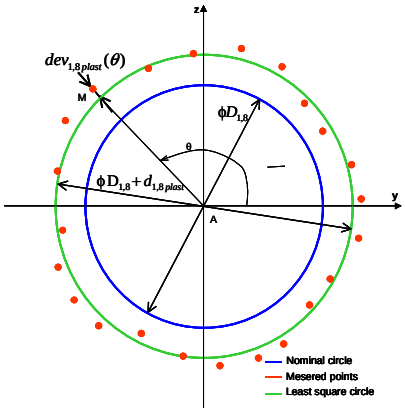

Figure 27: Plastic strain of surface 1,8 in plane $(A,\mathbf{x})$.

Three results in particular, which are similar to those found with behaviour II, characterise the distortion of surface 1,8 in plane $(A,\mathbf{x})$ see figure 27:

- the translation deviation at point A of the centre of the least square circle in relation to the centre of the nominal circle: $\varepsilon_{A,1,8/2,8plast} = 0$

- the diameter of the least square circle for the section under strain: $D_{1,8th} = D_{1,8} + d_{1,8plast}$

- the deviation in the form of the deformed section under strain: $dev_{1,8plast}(\theta)$

The thermomechanical deformation of surface 1,8 is not axisymmetrical.

We can deduce the Minkowski sum for hull $\mathfrak{D}_{1,8/2,8}$ characterising the displacement limits for surface 1,8 in relation to surface 2,8 for behaviour III: see figure 28.

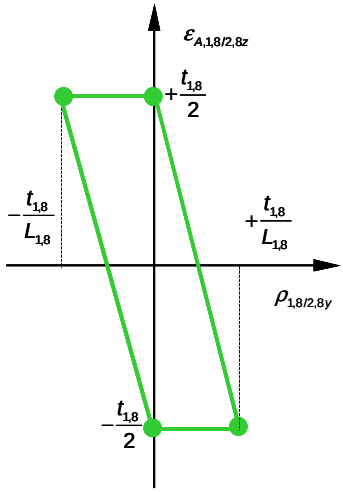

Figure 28: Hull $\mathfrak{D}_{1,8/2,8}$ at point A in behaviour III.

Equation (9), formalising fulfilment of the worst case FC condition in behaviour III, is the same as in behaviour II.

$$\left.\begin{aligned} e_{max} &\geq +\frac{t_{1,8}}{2} \\ e_{min} &\leq -\frac{t_{1,8}}{2} \end{aligned}\right\} \qquad (9)$$

Thus the translation deviation $b_{1,8}(\theta)$ from a point on the cylindrical surface 1,8 in relation to its nominal position takes plastic strains into account.

For behaviour situation I, see equation (10).

For behaviour situation II, see equation (11).

For behaviour situation III, see equation (12).

$$b_{1,8}(\theta) = \varepsilon_{A,1,8/2,8z} + \frac{D_{1,8} \pm d_{1,8}}{2} \quad (10)$$

$$b_{1,8}(\theta) = \varepsilon_{A,1,8/2,8z} + \frac{D_{1,8} + d_{1,8th} \pm d_{1,8}}{2} + dev_{1,8th}(\theta) \quad (11)$$

$$b_{1,8}(\theta) = \varepsilon_{A,1,8/2,8z} + \frac{D_{1,8} + d_{1,8plast} \pm d_{1,8}}{2} + dev_{1,8plast}(\theta) \quad (12)$$

In behaviour I, II and III, the limits of $\varepsilon_{A,1,8/2,8z}$ are given by the hulls of figures 19, 24 and 28 respectively.

4 CONCLUSIONS AND FUTURE PROSPECTS

We have shown how deviation hulls and clearance hulls can take into account thermomechanical and plastic strains in 3D dimension-chains.

This was put into application on a high-pressure turbine from a helicopter engine.

For a specific behaviour, the intervention of thermomechanical and plastic strains is in relation to a reference definition of the variability of geometric defects which corresponds to the behaviour of the system when new, integrating the effects of permanent strain which occur during the previous behaviour.

One of the main objectives of this study was to put forward qualification criteria for technical solutions envisaged in the design cycle of a high-pressure turbine using geometric specifications.

Another area for future study is to show the usefulness of considering different physical phenomena such as wear in certain joints and damage to some components, thus extending the definition of clearance to the tip of the blade and to the entire lifetime of a turbine.

Acknowledgements: This work was carried out within the framework of ERT 1070, joint research team of TREFLE-Turbomeca. Thanks to J.L. Breining, J. G. Senger and R. Thomas, of Turbomeca for their advice and technical assistance in carrying out this work.

5 REFERENCES

[1] Giordano, M., Duret, D., 1993, Clearance Space and Deviation Space, Application to three-dimensional chains of dimensions and positions, Proceedings of 3rd CIRP Seminar on Computer Aided Tolerancing, ISBN 2-212-08779-9, 179-196, Eyrolles.

[2] Giordano, M., Samper, S., Petit, J.P., 2005, Tolerance analysis and synthesis by means of deviation domains, axi-symetric cases. Proceedings of 9th CIRP Seminar on Computer Aided Tolerancing, ISBN 978-1-4020-5437-2, 85-94, Springer.

[3] Fleming A., 1988, Geometric relationships between toleranced features. Artificial Intelligent; 37 :403-412.

[4] Mujezinovi, A., Davidson, J-K., Shah, J-J., 2004, A new mathematical model for geometric tolerances as applied to round faces. ASME Transactions on Journal of Mechanical Design, 126:504–518.

[5] Jian A. D., Ameta G., Davidson J. K., Shah J. J., 2005, Tolerance Analysis and Allocation using Tolerance-Maps for a Power Saw Assembly Proceedings of 9th CIRP Seminar on Computer Aided Tolerancing, ISBN 978-1-4020-5437-2, 267-276, Springer.

[6] Teissandier, D., Delos, V., Couétard, Y., 1999, Operations on polytopes: application to tolerance analysis, Proceedings of 6th CIRP Seminar on Computer Aided Tolerancing ISBN 0-7923-5654-3, 425-433, Kluwer academic publisher.

[7] Stewart, M.-L., Chase, K.-W., 2005, Variation simulation of fixtured assembly for compliant structures using piecewise-linear analysis. American Society of Mechanical Engineers, Manufacturing Engineering Division, MED Volume 16-1:591-600.

[8] Söderberg, R., Lindkvist, L., Dahlström, S., 2006 Computer-aided robustness analysis for compliant assemblies. Journal of Engineering Design, 17:411–428.

[9] Cid, G., Thiebaut, F., Bourdet, P., Falgarone, H., 2005, Geometrical study of assembly behaviour, taking into accounts rigid components' deviations, actual geometric variations and deformations, Proceedings of 9th CIRP Seminar on Computer Aided Tolerancing, ISBN 978-1-4020-5437-2, 301-310, Springer.

[10] ISO 1101, 2005, Toleranced characteristics and symbols -- Examples of indication and interpretation.

[11] ISO 5459, 1981, Technical drawings -- Geometrical tolerancing -- Datums and datum-systems for geometrical tolerances.

[12] ISO 8015, 1985, Technical drawings -- Fundamental tolerancing principle.

[13] Ballu, A., Mathieu, L., 1999, Choice of functional specifications using graphs within the frame work of education. Proceedings of 6th CIRP Seminar on Computer Aided Tolerancing ISBN 0-7923-5654-3, 197-206, Kluwer academic publisher.

[14] Dantan, J.-Y., Mathieu, L., Ballu, A., Martin, P., 2005, Tolerance synthesis: quantifier notion and virtual boundary. Computer Aided Design; 37:231-240.

[15] Pierre, L., Teissandier, D., Nadeau, J.-P., 2008, Integration of thermomechanical strains into tolerancing analysis, Proceedings of IDMME2008, Beijing, October 8-10, China.